Filomat 39:17 (2025), 5965–5971
https://doi.org/10.2298/FIL2517965K

Published by Faculty of Sciences and Mathematics,
University of Niš, Serbia
Available at: http://www.pmf.ni.ac.rs/filomat

Numerical study of transonic flow in a channel at various back pressures

Alexander Kuzmin[a]

[a] *St. Petersburg State University, Russia*

Abstract. This paper addresses turbulent 2D airflow in a simple intake model. The numerical simulation is based on the system of Reynolds-averaged Navier–Stokes equations. Numerical solutions of the system are obtained with a finite-volume solver of second order accuracy on a fine computational mesh. The location of shock waves, across which flow parameters change abruptly, is analyzed at three supersonic inflow Mach numbers in a band of back pressure given at the exit of intake. The obtained solutions show the occurrence of non-uniqueness and self-excited oscillations. Transitions between different flow regimes are discussed. A comparison with experimental data available in the literature is made.

1. Introduction

Studies of high-speed airflow in curved or convergent-divergent channels are of practical interest, e.g, for the advanced design of supersonic aircraft engines. The efficiency of engine depends crucially on the geometry of intake in which the incoming atmospheric airflow decelerates to velocities suitable for fuel burning in the combustor. In on-design conditions, the deceleration of supersonic flow is accomplished through several oblique shock waves located inside and ahead of the intake. Meanwhile, in off-design conditions, when inflow Mach number M_∞ decreases or the pressure imposed at the exit pexit increases, the shock waves move upstream and eventually are expelled from the intake. The latter regime produces considerable losses in the engine efficiency.

A number of works addressed flow features in convergent-divergent intakes and bent channels under changes in freestream Mach number M_∞ or angle of attack α [5, 6, 8, 9]. Of significant importance is also the flow behavior under changes in the back pressure p_{exit} which can occur due to instability of processes in the combustor located downstream. An increase in back pressure can cause an unfavorable transition to a regime with an expelled shock wave. To prevent such a transition, the conventional intakes involve a sufficiently long part located downstream from the minimum cross section. Numerical simulation of flow regimes in a two-dimensional supersonic air intake under rapid changes in back pressure was performed in [12], where an influence of time and magnitude of pressure variation on flow characteristics was analyzed.

Zhao *et al.* [13] carried out an experimental study of the effect of back pressure on the flow in an intake model whose lower wall is 8° bent. A flow visualization by the Schlieren method and by the method of laser

2020 *Mathematics Subject Classification*. Primary 76H05; Secondary 76-10.
Keywords. Turbulent transonic flow, finite-volume solutions, non-uniqueness.
Received: 20 August 2024; Revised: 24 March 2025; Accepted: 28 Match 2025
Communicated by Ljubisa D. R. Kocinac
Email address: a.kuzmin@spbu.ru (Alexander Kuzmin)
ORCID iD: https://orcid.org/0000-0002-1699-9600 (Alexander Kuzmin)

scattering of nanoparticles showed the presence of a Mach configuration of shock waves and a significant separation of the boundary layer in all flow regimes. Also, an evident hysteresis was detected during an increase/decrease in the back pressure.

In this paper, we consider the same channel as in [13] and perform a numerical study of the stability of flow patterns at various Mach numbers M_∞ and back pressures p_{exit}.

2. Formulation of the problem and numerical method

Figure 1 shows a geometry of the intake model under consideration.

The turbulent 2D airflow is governed by the system of Reynolds averaged Navier–Stokes equations [11] with respect to static pressure $p(x, y, t)$, temperature $T(x, y, t)$, and velocity components $U(x, y, t)$, $V(x, y, t)$ in $x-$ and $y-$directions:

$$\rho_t + (\rho U)_x + (\rho V)_y = 0, \tag{1}$$

$$(\rho U)_t + (\rho U^2)_x + (\rho UV)_y = -p_x + \tau_x^{xx} + \tau_y^{xy}, \tag{2}$$

$$(\rho V)_t + (\rho UV)_x + (\rho V^2)_y = -p_y + \tau_x^{yx} + \tau_y^{yy}, \tag{3}$$

$$[\rho(c_v T + (U^2 + V^2)/2)]_t + [\rho U(c_p T + (U^2 + V^2)/2)]_x + [\rho V(c_p T + (U^2 + V^2)/2)]_y =$$
$$= (kT_x + U\tau^{xx} + V\tau^{xy} + \sigma^x)_x + (kT_y + U\tau^{yx} + V\tau^{yy} + \sigma^y)_y, \tag{4}$$

where (x, y) are the Cartesian coordinates, t is time, subscripts denote partial derivatives. The parameter k, vector (σ^x, σ^y) and tensor $(\tau^{xx}, \tau^{xy}, \tau^{yx}, \tau^{yy})$, which govern heat fluxes and turbulent viscosity, can be expressed in terms of U, V, p, T using a turbulence model.

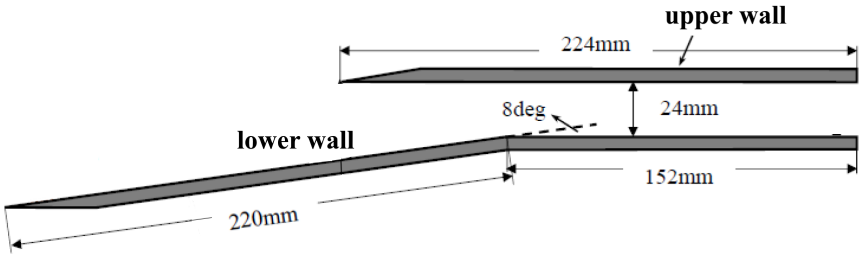

Figure 1: Geometry of the intake model [13].

Figure 2 illustrates the computational domain and mesh used. On the inflow boundary Γ_1 of the domain, we prescribe static pressure p_∞, Mach number M_∞, angle of attack $\alpha = 8°$, and temperature T_∞, which determine velocity components $U_\infty = M_\infty a_\infty \cos\alpha$, $V_\infty = M_\infty a_\infty \sin\alpha$, where $a_\infty = (\gamma R T_\infty)^{1/2}$ is the sound speed, $R = c_p - c_v$, $c_p = 1004.4$ J/(kg K) is specific heat at constant pressure, $c_v = c_p/\gamma$, $\gamma = 1.4$ is the ratio of specific heats. On the outflow boundary Γ_2 above the channel, we set the condition of supersonic flow velocity $M(x, y) > 1$. On the subsonic parts of the exit, we prescribe the static pressure p_{exit} and temperature $T_{\text{exit}} = 300°$. On the walls of channel, we set the no-slip condition and vanishing heat flux. Initial data in the computational domain is either the uniform freestream or flow field obtained for another value of p_{exit}.

The formulated initial-boundary value problem was solved numerically with an ANSYS-18.2 CFX finite-volume solver [1] on an unstructured mesh constituted by 758,528 elements. The elements were quadrilaterals in 38 layers on the walls, and triangles in the remaining region. The nondimensional thickness y^+ of the first mesh layer on the walls was less than 1. Test computations on a refined grid of approximately 1.2×10^6 cells only showed insignificant changes in the shock wave coordinates (less than 1.3 %). A global timestep of 2×10^{-6} s provided the root-mean-square Courant–Friedrichs–Lewy number smaller than 5. We employed a Shear Stress Transport $k - \omega$ turbulence model [7], which is based on two first-order partial differential equations with respect to the kinetic energy of turbulence and rate of eddies

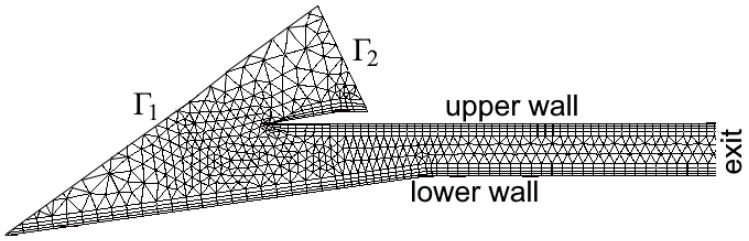

Figure 2: A schematic of the computational domain and mesh.

dissipation. This model is known to provide good accuracy of simulation of aerodynamic flows with boundary layer separation.

3. Results of the numerical simulation at $M_\infty = 2.7$

First, we considered the same inflow Mach number M_∞=2.7, velocity components U_∞=592.08, V_∞=83.21 m/s, temperature T_∞=122.1 K, and pressure p_∞=4,300 Pa, as in paper [13]. At p_{exit}=30,000 Pa, time-dependent numerical solutions demonstrated the convergence to a steady flow $p(x, y), T(x, y), U(x, y), V(x, y)$ in which there is a shock wave generated by the edge of upper wall, a shock wave SW emanated ahead of the lower wall corner, and a system of weak shocks between SW and the exit, see Fig. 3. Step-by-step increase in p_{exit} from 30,000 Pa to 32,500 Pa showed that the weak shocks gradually shift upstream, whereas SW persists; further increase in p_{exit} influences location of SW as well. The location of SW can be traced using its $x-$coordinate x_{sh} at the midheight of channel y = 42.6 mm, as pointed out in Fig. 3. If p_{exit} increases step-by-step from 32,500 Pa to 33,200 Pa, then the shock SW shifts upstream towards the entrance of channel; therefore, x_{sh} decreases, see Fig. 4. The step-by-step increase in p_{exit} implies that, at each step, initial data for computation of the solution is the flow field obtained at the previous step.

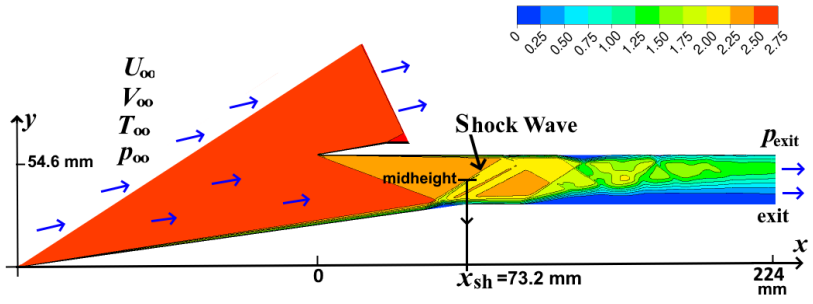

Figure 3: Mach number contours in the channel at M_∞=2.7, p_{exit}=30,000 Pa.

In the bands 33,200 < p_{exit}, Pa < 33,700 and 33,775 < p_{exit}, Pa ≤ 34,200 computations exhibit self-excited oscillations of the flow field in which x_{sh} oscillates between $x_{\text{sh,min}}$ and $x_{\text{sh,max}}$. Figure 5 shows that the oscillations are periodic and their frequency is 110 Hz.

At p_{exit} > 34,200 Pa, the shock SW shifts out of the channel and moves towards the inflow boundary of computational domain; in order to stabilize the location of SW in time, one needs to reduce p_{exit} to values smaller than 29,200 Pa as illustrated by the lower arrows in Fig. 4. Figure 6 demonstrates Mach number contours in the regime with an expelled shock at p_{exit}=29,000 Pa. As seen, the shock wave causes an essential boundary layer separation from the lower wall.

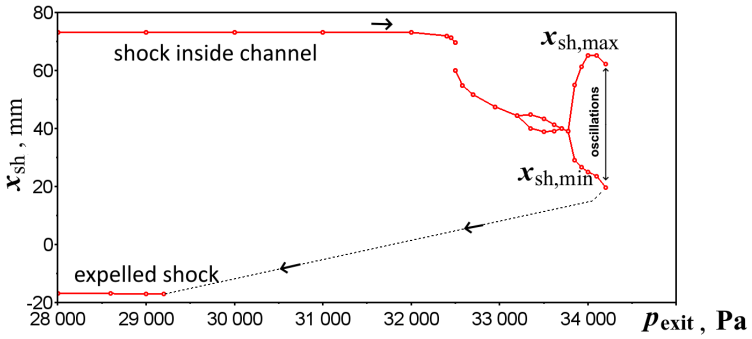

Figure 4: Dependence of the shock coordinate x_{sh} on p_{exit} at $M_\infty = 2.7$.

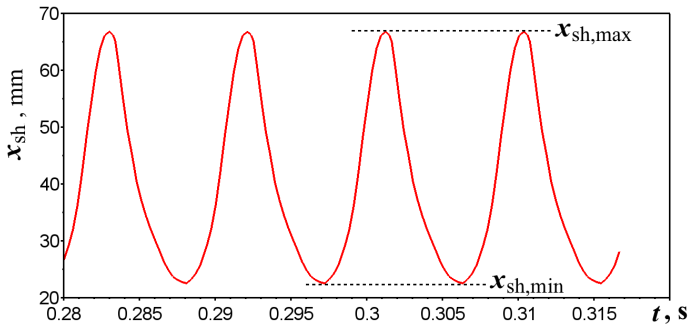

Figure 5: Oscillations of the shock coordinate x_{sh} in time at M_∞=2.7, p_{exit}=34,000 Pa.

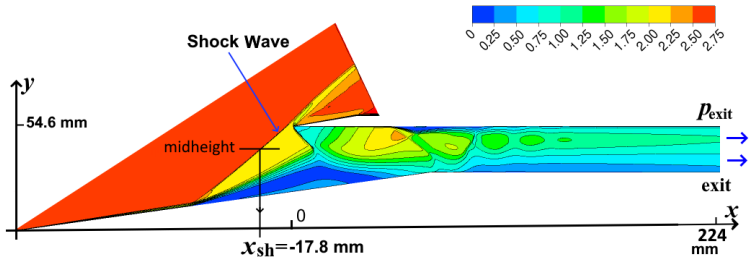

Figure 6: Mach number contours at p_{exit}=29,000 Pa in the flow regime with the shock wave expelled from channel.

The numerical simulations show that a transition from the lower branch of the curve $x_{sh}(p_{exit})$ in Fig. 4 to the upper branch, i.e., from the flow regime with the expelled shock to one with a swallowed shock (i.e., shock located inside the channel), cannot be performed through a decrease in p_{exit}. Such a transition can be triggered by an increase in the Mach number of the incoming flow M_∞ or pressure p_∞, followed by a return to the M_∞=2.7, p_∞=4,300 Pa.

The above presented results of the numerical study are in qualitative agreement with experimental data documented in paper [13], though periodic shock wave oscillations were not mentioned in [13]. We notice that our findings of the self-excited oscillations at large back pressures agree well with recent numerical results presented in [3, 10] where the oscillations in bent channels at large back pressures were detected as well.

4. Results of the numerical simulation at M_∞=2.6 and 2.5

In Section 2, the inflow static pressure and temperature p_∞, T_∞ were determined by M_∞=2.7 and the stagnation values p_0=101,000 Pa, T_0=300 K [13]. In this section, we retain p_0, T_0 and consider p_∞, T_∞ that correspond to smaller values of M_∞. In particular, for M_∞=2.6, isentropic relations [4] $p_\infty = p_0[1 + 0.5(\gamma - 1)M_\infty^2]^{-\gamma/(\gamma-1)}$, $T_\infty = T_0[1 + 0.5(\gamma - 1)M_\infty^2]^{-1}$ yield p_∞=5061.6 Pa, T_∞=127.6 K. Computations using these inflow parameters on the boundary Γ_1 and step-by-step changes in the back pressure revealed a dependence of the shock coordinate x_{sh} on p_{exit} that is depicted in Fig. 7. As seen, there is noticeable hysteresis created by the upper and middle branches of the curve $x_{sh}(p_{exit})$ in the band 36,300 < p_{exit}, Pa ≤ 37,500; also self-excited oscillations arise in the band 37,300 < p_{exit}, Pa ≤ 37,700.

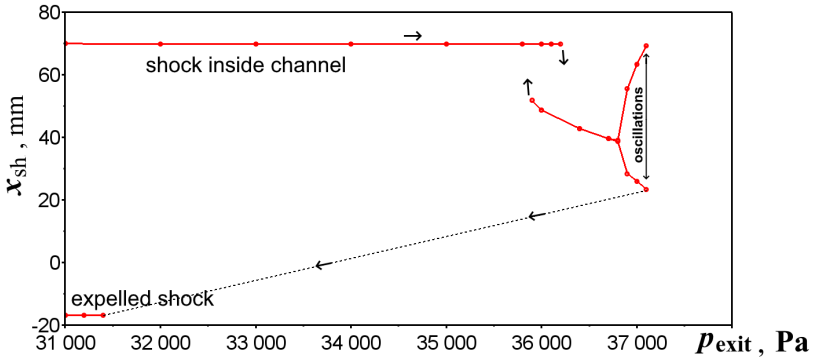

Figure 7: Dependence of the shock coordinate x_{sh} on the back pressure p_{exit} at M_∞ = 2.6.

For M_∞=2.5 and the same stagnation parameters p_0=101,000 Pa, T_0=300 K, isentropic relations [4] yield T_∞=133.3 K, p_∞=5911.3 Pa. Numerical simulations using these inflow parameters and step-by-step changes in p_{exit} produced a dependence of the shock coordinate xsh on p_{exit} that is illustrated by Fig. 8. As seen, in the band 39,280 ≤ p_{exit}, Pa ≤ 40,150 there exist two different flow regimes with different locations of shock wave SW in the channel. The non-uniqueness is attributed to nonlinear phenomena associated with an essential boundary layer separation from the lower wall. The realization of a certain regime depends on the time history of variations in p_{exit}.

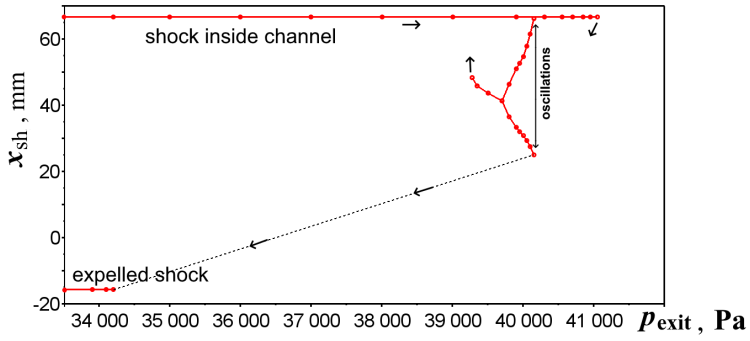

Figure 8: Dependence of the shock coordinate x_{sh} on the back pressure pexit at M_∞=2.5.

We mention that if one sets M_∞=2.5 and the same T_∞=122.1 K, p_∞=4,300 Pa as in the case M_∞=2.7 (such a setting implies changes in the stagnation values), then numerical simulations show a dependence $x_{sh}(p_{exit})$ that looks similar to the one in Fig. 8, though the middle branch of the curve shrinks to a very short interval 28,500 ≤ p_{exit}, Pa ≤ 29,000 instead of 39,280 ≤ p_{exit}, Pa ≤ 40,150.

5. Computation of total pressure losses

Using the obtained distributions $M(x, y), p(x, y)$, one can calculate the total pressure in the flow with the expression [2]

$$p_{\text{total}}(x, y) = p(x, y)[1 + 0.5(\gamma - 1)M^2(x, y)]^{\gamma/(\gamma-1)}. \quad (5)$$

The total pressure is known to remain constant along a streamline in inviscid flow until the streamline intersects a shock wave. On the shock, the total pressure experiences a drop/loss whose amount depends on the shock strength. For convenience, instead of (5) we use the relative total pressure $p_{\text{total,relat}} = p_{\text{total}}/p_0$. Figure 9 displays distributions of $p_{\text{total,relat}}$ at M_∞=2.5, p_{exit}=34,200 Pa in the regimes with swallowed and expelled shock waves, which correspond to the upper and lower branches of the curve in Fig. 8, respectively. It can be seen that, the regime with an expelled shock admits are significant losses in p_{total} which lead to losses in the efficiency of the airbreathing engine in practice, as mentioned above in Introduction.

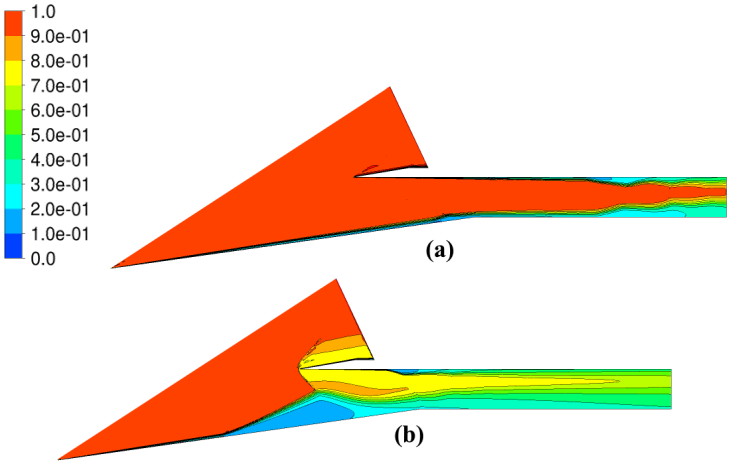

Figure 9: Relative total pressure $p_{\text{total,relat}}$ in the channel at M_∞=2.5, p_{exit}=34,200 Pa in the regimes with (a) swallowed and (b) expelled shock waves.

6. Conclusion

For the inflow Mach number M_∞=2.7, the numerical solutions demonstrated qualitative agreement of flow patterns in the intake with those documented in experiments [13]. The solutions made it possible to trace locations of the shock wave SW generated ahead of the corner of lower wall at various back pressures p_{exit}. Self-exciting oscillations of SW are detected at back pressures close to the upper bound p_{exit}=34,200 Pa of the considered pressure interval. The development of oscillations is in agreement with well-known phenomenon: "As the back pressure of the inlet increases . . . the shock train moves forward"; eventually, "the shock position will move forward and backward, presenting a state of self-excitation oscillation" [3]. Larger back pressures $p_{\text{exit}} > 34{,}200$ Pa trigger an expulsion of SW from the intake; in this case one needs to reduce essentially p_{exit} in order to stabilize SW location.

At the smaller inflow Mach numbers M_∞=2.6, 2.5, the numerical solutions exhibited a noticeable non-uniqueness/hysteresis in the regimes with SW located in the intake.

The crucial role of the boundary layer separation shows a distinction of the problem at hand from a similar problem at M_∞=1.6 - 1.8 [6], where flow instability and non-uniqueness are caused by an interaction of the shock wave generated by the leading edge of upper wall with the expansion flow region over the corner of lower wall.

Acknowledgements

This research was performed using computational resources provided by the Computational Center of St. Petersburg State University (http://cc.spbu.ru).

References

[1] ANSYS Fluids - Computational Fluid Dynamics. https://www.ansys.com/products/fluids (accessed: 18.05.2024).
[2] O. Biblarz, R. D. Zucker, *Fundamentals of Gas Dynamics*, 3rd edition, Wiley, Hoboken, New Jersey, U.S., 2019.
[3] F. Cai, X. Huang, *Study on self-excited oscillation suppression of supersonic inlet based on parallel cavity*, Front. Energy Research **10** (2022), 1–15.
[4] Compressible Aerodynamic Calculator, https://devenport.aoe.vt.edu/aoe3114/calc.html (accessed: 18.05.2024).
[5] T. Cui, Y. Wang, K. Liu, J. Jin, *Classification of combustor-inlet interactions for airbreathing ramjet propulsion*, AIAA Journal **53** (2015), 2237–2255.
[6] A. Kuzmin, *Non-unique regimes of oscillatory transonic flow in bent channels*, Aerospace Syst. **7** (2024), 493–499.
[7] F. R. Menter, *Review of the shear-stress transport turbulence model experience from an industrial perspective*, Int. J. Comput. Fluid Dyn. **23** (2009), 305–316.
[8] N. Mushtaq, P. Gaetani, *Understanding and modeling unstarting phenomena in a supersonic inlet cascade*, Physics of Fluids **35** (2023), Article ID 106101, 1–22.
[9] D. Panchal, D. Chayani, *Review paper on the unstarting of the supersonic air intake*, Int. J. Eng. Research Technology **10** (2021), 11–15.
[10] A. L. Philippou, P. K. Zachos, D. G. MacManus, *Aerodynamic instabilities in high-speed air intakes and their role in propulsion system integration*, Aerospace **11** (2024), 1–50.
[11] H. Tennekes, J. L. Lumley, *A First Course in Turbulence* (14th ed.), MIT Press, Cambridge, 1992.
[12] K. Wang, J. Y. Wang, H. X. Huang, L. R. Xie, Y. Liu, H. J. Tan, *Effects of backpressure on unstart and restart characteristics of a supersonic inlet*, The Aeronautical J. **127** (2023), 1774–1792.
[13] Y. L. Zhao, Y. Y. Zhou, Y. X. Zhao, *Experimental study of the unstart/restart process of a two-dimensional supersonic inlet induced by backpressure*, J. Appl. Fluid Mechanics **15** (2022), 415–426.